SPACE TELESCOPE SCIENCE INSTITUTE
Operated for NASA by AURA

Instrument Science Report WFC 2012-07

WFC3/UVIS and IR Multi-Wavelength Geometric Distortion

V. Kozhurina-Platais, M. Dulude,

T. Dahlen, C. Cox

April 30, 2012

Abstract

Standard astrometric catalog based on ACS/WFC observations of the globular cluster ω Cen field has been utilized to examine the geometric distortion of WFC3/UVIS and IR as a function of wavelength. The observations of this field were taken with large dither patterns and a wide range of HST roll-angles exposed through 13 UVIS and 8 IR band-passes. A 4^{th} order polynomial model was used to derive the UVIS and IR geometric distortion coefficients relative to the distortion free coordinates of the astrometric field. The main result of these calibrations are: 1) geometric distortion can be successfully corrected at the 0.1 pixels (2 and 7 mas) precision level in UVIS and IR channels, respectively; 2) the UVIS relative scale changes from filter to filter by ∼0.02%; 3) the IR relative scale is nearly constant from filter to filter; 4) the unique polynomial coefficients of the geometric distortion in the 13 UVIS and 8 IR filters are used in the STScI reprocessing pipeline to correct WFC3 images for distortion.

1. Introduction

Wide Field Camera 3 (WFC3), a fourth-generation imaging instrument on-board *HST*, was installed during Servicing Mission 4 in May 2009. By design, the focal plane

arrays of the WFC3/UVIS and IR cameras are tilted with respect to the incoming beam at $\sim$21° and $\sim$24°, respectively. As a result, the WFC3/UVIS and IR images are distorted by an amount of $\sim$ 7% across the detector, which corresponds to a maximum of 120 pixels or $\sim$5″ in the UVIS and 35 pixels or $\sim$4″ in the IR channel.

Accurate knowledge of the geometric distortion is important not only for deriving precise positions, parallaxes and proper motions of scientifically interesting objects, but also to rectify WFC3 images. The Multidrizzle software (Koekemoer 2002; Fruchter & Hook, 2002; Fruchter *et al.* 2009), currently used by the STScI on-the-fly reprocessing pipeline (OTFR), requires accurate distortion correction in order to combine dithered WFC3 images (UVIS and IR), to enhance the spatial resolution, and to deepen the detection limit. If the geometric distortion correction as implemented in Multidrizzle is not accurate enough, then the image combination can produce blurred images and distort the under-sampled Point Spread Function (PSF).

Right after Servicing Mission 4, the astrometric calibrations of WFC3/UVIS & IR were based on two astrometric standard fields, one in the globular cluster 47 Tuc (Anderson, 2007) and the other in the Large Magellanic Cloud (Anderson, 2008). Both fields were observed with the F606W UVIS and F160W IR filters, and with different dither patterns. The derived WFC3/UVIS & IR geometric distortion models, as described in Kozhurina-Platais *et al.* (2009a, 2009b), are represented by fourth-order polynomial models and are accurate to the level of $\lesssim$0.1 pixel, corresponding to 2 and 7 *mas*) in the UVIS and IR channels, respectively.

In Cycle 18, with observations starting in July 2009, a standard astrometric catalog based on ACS/WFC observations of the globular cluster ω Cen field was used to examine the multi-wavelength geometric distortion of WFC3/UVIS and IR channels, thus, expanding the investigation from the previous solutions that were based on a single filter for each camera. To do this, the globular cluster ω Cen was observed through 10 UVIS and 5 IR filters (CAL–11911, PI E. Sabbi, CAL–11928, PI V.Kozhurina-Platais) . The new coefficients of the geometric distortion in 10 UVIS and 5 IR filters derived from these programs have been used in the OTFR since March-April 2011. In Cycle 19, (CAL–12353, PI Kozhurina-Platais) ω Cen was observed in 3 additional UVIS and IR filters. These new additional calibrated filters were delivered to OTFR in March 2011. Thus, the new calibrated 3 UVIS and 3 IR filters have expanded the WFC3 individual geometric solutions to 13 UVIS and 8 IR filters.

Here, we present the analysis and results of the multi-wavelength geometric distortion calibration. The final precision is of the level of $\lesssim$0.1 pixels (or 2 and 7 *mas* respectively), which is sufficient to combine dithered and mosaicked WFC3 UVIS and IR multi-filter images using the STSDAS Multidrizzle software. The derived coefficients of geometric distortion in the UVIS and IR channels are represented in the form of a reference file called Instrument Distortion Correction Table (IDCTAB, Hack & Cox, 2001).

2. Observations

The standard astrometric catalog in the vicinity of the globular cluster ω Cen, which is a rectangular coordinate system free of any systematics in the positions (Anderson 2009), was used for a multi-wavelength geometric distortion calibration of the UVIS and IR channels. The tangent–plane projection type positions (hereafter the U, V) of stars in the standard astrometric catalog are globally accurate to ∼0.02 ACS/WFC pixels or 1 *mas* (Anderson & van der Marel, 2010). The globular cluster ω Cen was observed in Cycle 18 with the UVIS and IR detectors near the center of the standard astrometric catalog with a large dither pattern ($\pm$ 40″ and $\pm$ 31″ for UVIS and IR, respectively) and at different HST roll-angles (CAL–11911, PI–E. Sabbi and CAL–11928, PI–V. Kozhurina-Platais) and over a 2–year time baseline. The observations were taken through 10 UVIS filters and 5 IR filters. During the second epoch observations (CAL-11911, April 2010), there was a problem with a guide star acquisition and, because of that, several images in certain UVIS filters were lost and recovered later, thus yielding to have an additional images for calibration. In Cycle 19 (CAL-12353 PI Kozhurina-Platais), the observations of ω Cen were taken at two epochs through additional 3 UVIS and 3 IR filters. In each epoch, ω Cen was observed through each filter with different HST roll-angles and without dithering. Appendix A (Tables 1 & 2) lists all observations of ω Cen though the 13 UVIS and 8 IR filters.

3. Reductions

The reductions and analysis to derive multi–wavelength geometric distortion calibration for the UVIS and IR channels are similar to the reductions and analysis used in the SMOV UVIS and IR geometric distortions calibrations, described in detail by Kozhurina-Platais *et al.*, (2009a, 2009b). At the time of our analysis, high precision tools, such as an *effectivePSF* library like the one derived for the ACS/WFC camera (Anderson, 2002), were only available in the IR. In UVIS, the IRAF/DAOPHOT/PHOT task with CENTERPARS, which includes a 2D-Gaussian fit to the PSF and which simultaneously performs aperture photometry, was used to obtain the X & Y positions of stars on each of the UVIS CCD chips and each UVIS filter. As seen in Figure 1, a Gaussian fit to X and Y positions derived from single `*_flt.fits` UVIS images in F606W filter as a function of instrumental magnitude, provides a reasonable good formal measuring precision even for the under-sampled UVIS PSF. Here the errors represent the centering errors of the Gaussian fit performed by CENTERPARS. The instrumental magnitude is defined as $Inst.mag = -2.5log10(FLUX/EXPTIME)$, where $FLUX$ is the signal from a star (in e^-) as given by the formalism of aperture photometry, and $EXPTIME$ is the exposure time in seconds.

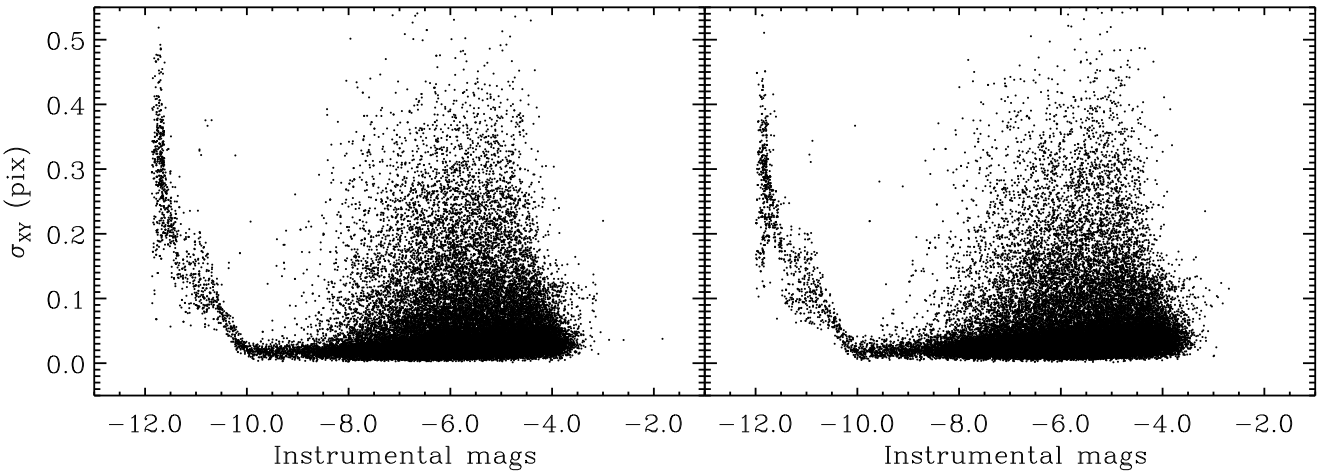

Fig. 1.— Formal centering errors of X & Y positions as a function of instrumental magnitude for stars from a single UVIS image of ω *Cen* (UVIS1 and UVIS2 CCD chip left and right panel, respectively). The points above the trend of astrometric error in UVIS ($\sigma_{XY} \gtrsim 0.1$ for -10.0 $\lesssim$ mag $\lesssim$ -4) are likely to be cosmic rays, blended and spurious detections. The stars brighter than about -10 magnitude are saturated. Position errors (σ_{XY}) are calculated as $\sqrt{(\sigma_X^2 + \sigma_Y^2)}$

.

Nearly 40,000 stars in each UVIS CCD image that have the formal errors on or below the astrometric error trend (see Figure 1) and were considered to be accurately measured.

In the IR, an *ePSF* library was available (Anderson, 2010) at the time of IR analysis, thus, the *ePSF* fitting technique was used to obtain accurate and high-precision X & Y positions of stars in each of the IR images. Figure 2 shows a quality–of–fit parameter QU to X & Y positions as a function of IR instrumental magnitude for stars from a single F106W IR image. The quality–of–fit parameter is defined by the formalism of ePSF fitting (Anderson & King, 2006).

About 6,000 stars in each IR image with the errors on or below the astrometric error trend (see Figure 2) were considered as well-measured.

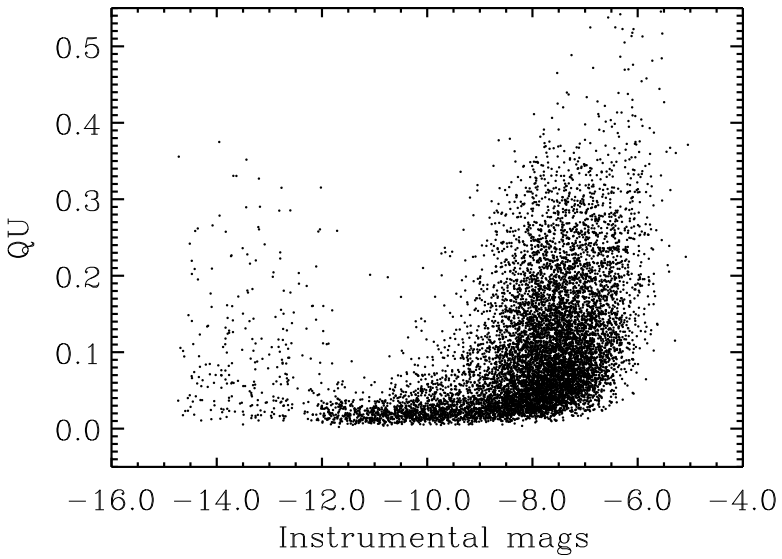

Fig. 2.— Formal centering errors of X & Y positions as a function of instrumental magnitude, for stars from a single F160W IR image of ωCen. The points above the trend of QU in IR ($QU \gtrsim 0.1$ for -12.0 $\lesssim$ mag $\lesssim$ -6) are likely to be blended or spurious detections. The stars brighter than about -12 magnitude are saturated. QU is the quality–of–fit parameter defined by the ePSF fitting formalism.

4. Analysis

4.1. Polynomial Solutions.

Similar to the SMOV calibration (Kozhurina-Platais *et al.*, (2009a, 2009b)), a fourth–order polynomial was used to derive the coefficients of geometric distortion for UVIS and IR, namely:

$$U = A_1 + A_2X + A_3Y + A_4X^2 + A_5XY + A_6Y^2 + A_7X^3 + ... + A_{15}Y^4 \quad (1)$$

$$V = B_1 + B_2X + B_3Y + B_4X^2 + B_5XY + B_6Y^2 + B_7Y^3 + ... + B_{15}Y^4 \quad (2)$$

where U & V are the tangent–plane positions in our astrometric standard catalog, and X & Y are the measured pixel positions in the observed UVIS or IR frame. Independent geometric distortion solutions were calculated using the least–squares minimization of the fourth -order polynomial by solving for the 15 parameters in Eq. (1) and Eq (2). This was done for each of the two UVIS CCD chips and for 13 UVIS filters and for 8 filters in the IR detector.

It is important to mention here that during each least-squares solution cosmic rays, saturated stars, hot pixels and spurious detected objects were interactively rejected from solutions as extreme outliers with large residuals ($\gtrsim$ 0.1 pixels). A total of 5–10% of detected objects were rejected during this interactive process. These numbers vary from one image to another depending on the degree of overlap between the U & V and X & Y systems of coordinates. Thus, about 40,000 stars were detected in each of the UVIS CCD chips and about 6,000 stars were detected in IR frames from ω Cen observations – a sufficient number to properly model the geometric distortion with a high-order polynomial.

The RMS of these solutions were about 2 *mas* and 7 *mas* in UVIS and IR, respectively. It is interesting to note, that the RMS of the solutions is a factor of three larger than the RMS of 0.8 *mas* from the Large Magellanic Cloud (LMC) solution, used in SMOV calibration. A simple explanation for such a high RMS is an unaccounted intrinsic dispersion of the proper motions of ω Cen. According to Dinescu *et al.*, (1999), the absolute proper motion of ω Cen are $\mu_\alpha cos\delta$=−4.9 *mas* and μ_δ=−3.5 *mas* per year. However, this systematic motion of the cluster contributes only to the constant terms A1 and B1, which have no influence on various high-order terms, defined by Eqs.1–2. A significant contribution to the terms and the RMS scatter of solutions would make not this absolute motion, but the substantial internal velocity dispersion in the proper motions of ω Cen, equal to 0.9 *mas* per year (Anderson & van der Marel 2010). This dispersion scales up proportionally to the epoch difference. Hence, the epoch difference of four years contributes to the RMS of the solution as much as ∼4 *mas* and ∼7 *mas* or 0.1 UVIS and IR pixels respectively, which corroborate the actual measured RMS.

The fourteen sets of coefficients (A_2–A_{15} and B_2–B_{15}) from each individual least-square

minimizations of the fourth order polynomial were averaged and the standard deviation of the coefficients calculated for each UVIS and IR filter, considered for calibration.

The different terms in the general polynomial characterize separate components of the geometric distortion. For example, in the X solution: the A_7 through A_{15} terms in the general polynomial are classical cubic- and fifth-order distortion terms: the 3rd–order terms indicate the presence of a pin–cushion type of distortion; and the 5th-order terms would indicate the presence of a barrel–type of distortion. Specifically to our solution, the 4th-order terms (the terms A_7 through A_{15}, Eq. 1-2) indicate the distortion between the pin-cushion and the barrel type; while the 2nd order terms, A_4 and A_5, are the plate tilt terms (van de Kamp, 1967); the linear terms, A_2 and B_3, are most significant and represent the relative plate scale in X and Y.

Thus, as a result of the UVIS and IR multi-wavelength geometric distortion calibration, for each of the 13 observed UVIS filters and 8 observed IR filters, unique polynomial coefficients were obtained which accurately represent the geometric distortion in UVIS and IR filters.

4.2. UVIS Multi–Wavelength Distortion.

As described above, the linear terms A_2 and B_3 in Eq. 1–2 are most significant and represent the relative plate scale in X and Y. In order to characterize the filter dependency of the distortion, the linear coefficients A_2 and B_3 (Eq.1–2) from the F606W UVIS solutions were chosen as a reference scale. Then, the same linear coefficients from the solutions in the other filters were compared to the F606W linear coefficients, namely:

$$\Delta X_{scale} = (X_{F606W} - X_{Filter}) \times S \quad (3)$$

$$\Delta Y_{scale} = (Y_{F606W} - Y_{Filter}) \times S \quad (4)$$

where X_{F606W} and Y_{F606W} are the linear terms A_2 and B_3 from the UVIS F606W solution and X_{Filter} and Y_{Filter} are the linear terms from the appropriate filter solution and S is the scale which provides the size of the effect in pixels at the far edge of UVIS detector (S=2048 pixels, half of the detector size).

Figures 3 and 4 show the maximum displacement in UVIS1 and UVIS2 CCD chips due to the plate scale difference compared to the F606W filter.

As seen from these figures, the amount of the linear geometric distortion (the plate scale) varies as a function of wavelength. For example, the difference in the scale in F225W filter is larger by ∼0.02% than in the F606W filter. However, the scale difference in the F390W filter is ∼0.01% smaller relative to F606W.

Similar filter–dependent distortions are reported in WFPC2 filters by Trauger *et al.* (1995). For example, Kozhurina-Platais *et al.* (2003) showed that for WFPC2, the scale

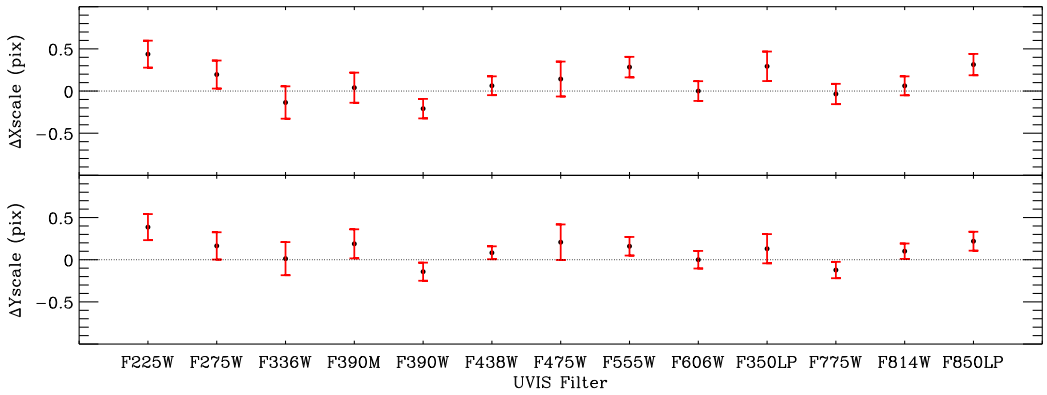

Fig. 3.— UVIS1 relative plate scale displacement with respect to F606W filter. The upper and lower panels show the plate scale in X and Y for the UVIS1 CCD chip. The over-plotted error bars show the errors of X and Y scale respectively. The scaling by 2048 provides the size of the effect in pixels at the far edge of UVIS detector.

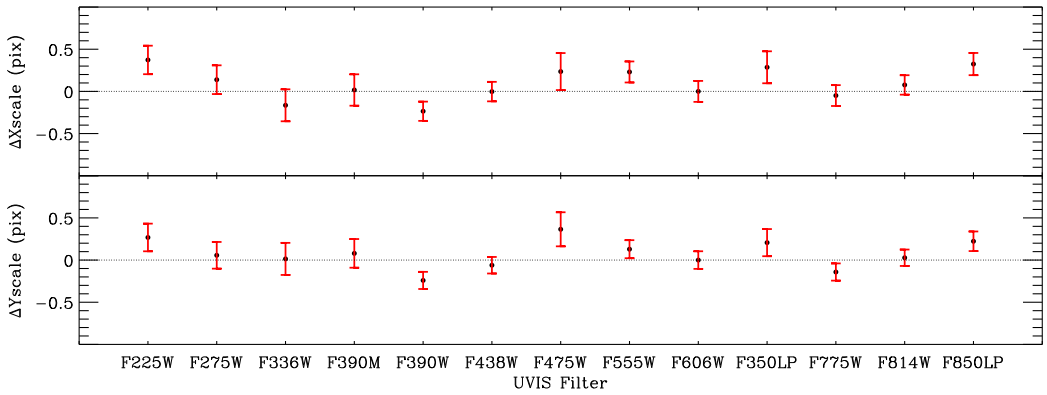

Fig. 4.— The same as Fig.3 but for the UVIS2 CCD chip.

difference in F300W filter is 0.5% larger than in F555W, but in F814W it is 0.3% smaller than in F555W.

The variations of the plate scale as a function of wavelength seen in Figures 3 & 4 are in good agreement with the results of the independent UVIS geometric distortion calibrations by Bellini *et.al* (2011, see Fig. 9), where the relative plate scale for UVIS filters also exhibits some semi–periodic trend as a function of wavelength.

The main reason for the variation in the UVIS plate scale as a function of wavelength is a variation in the thickness of a filter itself, which is especially significant in the UV filters. As discussed by Sabbi (2012), the variation in the thickness of a filter modifies the

distribution of the light beam, and, as a result, introduces a plate scale change and the offset in the centroid of a stellar object with respect to other filters. Also, Sabbi (2012) found that the largest offsets in the positions with respect to the F606W are in the F775W and the F850LP filters. For example, as seen in Figure 3–4, the Y scale in the F775W filter is smaller by ∼0.02% than in the F606W filter, while the F775W filter X scale is equal to the F606W filter X scale. Because of the noted differences in the UVIS plate scale as a function of wavelength, the coefficients for an uncalibrated UVIS-filter can be adopted as those from the nearest of the thirteen calibrated filters.

4.3. IR Multi–Wavelength Distortion.

In order to characterize the IR filter dependency distortion, the linear coefficients A_2 and B_3 (Eq.1–2) from F160W IR solutions were chosen as a reference scale. Similar to UVIS, the linear coefficients from the solutions in the other filters were compared to the reference F160W linear coefficients:

$$\Delta X_{scale} = (X_{F160W} - X_{Filter}) \times S \quad (5)$$

$$\Delta Y_{scale} = (Y_{F160W} - Y_{Filter}) \times S \quad (6)$$

where X_{F160W} and Y_{F160W} are the linear terms A_2 and B_3 from the IR F160W solution and X_{Filter} and Y_{Filter} are the linear terms from the chosen filter solution and S is the scale which provides the size of the effect in pixels at the edge of the IR detector (S=512 pixel).

Figure 5 shows the maximum displacement in IR detector due to the scale change with respect to the F160W filter.

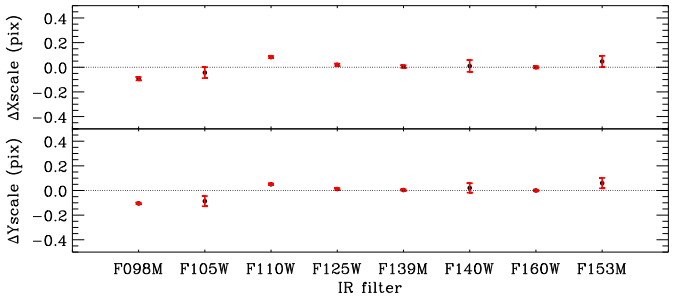

Fig. 5.— IR relative plate scale displacement with respect to F160W filter. The upper and lower panels show the scale in X and Y for the IR detector. The scaling by 512 provides the size of the effect in pixels at the edge of IR detector. The error bars are small compared to the actual scale difference.

As seen from Figure5, the relative IR plate scale deviations from filter to filter is small and quite stable (with the exception of F098M, F110W filters). The difference in the plate scale in the F098M filter is smaller by ∼0.02% than in the F160W filter, while the difference in the scale in the F110W filter is larger by ∼0.02% than in the F160W filter.

There is a clear indication that the amount of the IR linear geometric distortion from filter to filter remains nearly constant. Therefore, it is safe to adopt the distortion coefficients from the F160W filter for the other uncalibrated IR filters.

5. Conclusion

Two years of observation of ω Cen with UVIS and IR filters have been used to examine the WFC3/UVIS and IR geometric distortion as a function of wavelength. For each of the 13 observed UVIS filters and 8 observed IR filters, unique polynomial coefficients were obtained which accurately represent the geometric distortion. The derived geometric distortion coefficients in the form of IDCTAB can be successfully used in STSDAS/Multidrizzle software for: 1) stacking of WFC3/UVIS and IR images with different dither pattern and orientation; 2) rejecting the CRs; 3) enhancing the spatial resolution; 4) deepening the detection limit. The geometric distortion can be successfully corrected at the level of less than 0.1 pixels or 2 and 7 *mas* precision level in UVIS and IR images, respectively.

Summarizing the multi-wavelength geometric distortion for WFC3/UVIS, we conclude that the plate scale in the adopted distortion model varies as a function of UVIS filter. This variation apparently is due to the differences in the physical thickness of the WFC3/UVIS filters. Because of that, the coefficients for an uncalibrated UVIS-filters can be adopted from the nearest in central wavelength of the thirteen calibrated filters.

The next step in the improvement of UVIS geometric distortion should be the implementation of a look-up table (DGEO file) in Multidrizzle software to remove the fine–scale variations due to photo-lithography pattern in the WFC3/UVIS images.

In the IR, we note that the precision level in IR distortion mainly depends on the accuracy of the centering technique for measuring the X and Y positions of the severely under-sampled PSF on drizzled IR images. However, the deviations of the plate scale from filter to filter are quite stable and small within the measurement errors, which indicates that the amount of the IR linear geometric distortion remains nearly constant. Therefore, it is safe to adopt the distortion coefficients from the F160W filter for the other uncalibrated IR filters.

Acknowledgments

V.K.-P. is grateful to Jay Anderson for sharing his IR ePSF library and PSF fitting software. V.K.-Platais greatly express the gratitude to Jennifer Mack for the extensive

tests of the UVIS and IR IDCTABs. We gratefully appreciate L. Petro for his keen interest and valuable comments in the different stages of the WFC3/UVIS & IR geometric distortion calibration campaign. We are grateful to the referee, Elena Sabbi, for a number of suggestions that considerably improved the quality of the paper.

References

Anderson, J., King, I., 2006, ACS Instrument Science Report, ACS-ISR-06-01, (Baltimore:STScI)

Anderson, J., 2007, ACS Instrument Science Report, ACS-ISR-07-08 (Baltimore:STScI)

Anderson, J., 2008, in private communication

Anderson, J., 2009, in private communication

Anderson, J., 2010, in private communication

Anderson, J., & van der Marel, R.P., 2010, ApJ, 710, 1032-1062

Dinescu, D., van Altena, W.,F., Girard, T.M., Lopez, K., 1999, ApJ, 117, 277-285

Fruchter, A., Hook, P., 2002, PASP, v.114,pp.144-152

Fruchter A., Sosey, M., et.al, 2009, in " The MultiDrizzle Handbook", v.3, (Baltimore:STScI)

Hack, W., Cox, C., 2001, ACS Instrument Science Report, ACS-ISR-01–08, (Baltimore: STScI)

Koekemoer, A.,M., Fruchter, A., Hook, R.,N., Hack, W., 2002, in "2002 HST Calibration Workshop", eds A.Arribas, A. Koekemoer, B.C, Whitmore, (Baltimore:STScI), p.337

Kozhurina-Platais, V., Cox, C., McLean, B., Petro, L., Dressel, L., Bushouse, H., Sabbi, E., 2009a, WFC3 Instrument Science Report, WFC3-ISR - 09–33, (Baltimore:STScI)

Kozhurina-Platais, V., Cox, C., McLean, B., Petro, L., Dressel, L., Bushouse, H., 2009b, WFC3 Instrument Science Report, WFC3-ISR - 09–34, (Baltimore:STScI)

Kozhurina-Platais, V., Cox, C., Petro, L., Dulude, M., Mack, J., 2010, in "2010 HST Calibration Workshop", eds S. Deustua, C. Oliveira (Baltimore:STScI)

Sabby, E., 2012, WFC3 Instrument Science Report, WFC3-ISR - 2012–01, (Baltimore:STScI)

Trauger, T.T., Vaughan, A.H., Evans, R.W., Moddy, D.D., 1995, in "Calibrating Hubble Space Telescope: Post Servicing Mission", eds Koratkar, A., Leitherer, C., (Baltimore:STScI)

van de Kamp, P., 1967, "Principles of Astrometry", by W. H. Freeman & Company (San Francisco and London)

Appendix A

Table 1: UVIS Observation of ωCen

Date yy-mm-dd	α (°)	δ (°)	POSTARGS (″)	PA_V3 (°)	Filter	Exp.Time (sec)	Number of Images
2009-07-15	201.6983	-47.4795	±40	286.8	F225W	350	9
	201.6983	-47.4795	±40	286.8	F275W	350	9
	201.6983	-47.4795	±40	286.8	F336W	350	9
2010-01-14	201.6928	-47.479	±40	105.0	F225W	900	9
	201.6928	-47.4791	±40	105.0	F275W	800	9
	201.6928	-47.4791	±40	105.0	F336W	350	9
	201.6928	-47.4791	±40	105.0	F390W	350	9
	201.6928	-47.4791	±40	105.0	F438W	350	9
	201.6928	-47.4791	±40	105.0	F555W	40	9
	201.6928	-47.4791	±40	105.0	F606W	40	9
	201.6928	-47.4791	±40	105.0	F775W	350	9
	201.6928	-47.4791	±40	105.0	F814W	40	9
	201.6928	-47.4791	±40	105.0	F850LP	60	9
2010-04-29	201.6928	-47.4791	±40	199.9	F225W	900	5
	201.6928	-47.4791	±40	199.9	F275W	900	4
	201.6928	-47.4791	±40	199.9	F336W	350	1
	201.6928	-47.4791	±40	199.9	F390W	350	5
2010-04-29	201.6928	-47.4791	±40	199.9	F438W	350	7
	201.6928	-47.4791	±40	199.9	F555W	40	9
	201.6928	-47.4791	±40	199.9	F606W	40	9
	201.6928	-47.4791	±40	199.9	F775W	350	7
	201.6928	-47.4791	±40	199.9	F814W	40	6
	201.6928	-47.4791	±40	199.9	F850LP	60	5
2010-06-30	201.6828	-47.4791	±40	279.9	F275W	800	9
	201.6828	-47.4791	±40	279.9	F336W	350	9
	201.6828	-47.4791	±40	279.9	F438W	350	9
	201.6828	-47.4791	±40	279.9	F606W	40	9
	201.6828	-47.4791	±40	279.9	F814W	40	9
2010-12-12	201.6828	-47.4791	0	83.18	F390M	350	2
	201.6828	-47.4791	0	83.18	F350LP	350	2
	201.6828	-47.4791	0	83.18	F475W	350	1
2011-07-11	201.6828	-47.4791	0	275.99	F390LP	350	2
	201.6828	-47.4791	0	275.99	F390M	350	2
	201.6828	-47.4791	0	275.99	F475W	350	1

Table 2: IR Observations of ωCen

Date yy-mm-dd	α (°)	δ (°)	POSTARGS (″)	PA_V3 (°)	Filter	Exp.Time (sec)	Number of Images
2009-12-10	201.6828	-47.4791	±31	85.9	F098M	352.9	9
	201.6828	-47.4791	±31	85.9	F110W	227.9	9
	201.6828	-47.4791	±31	85.9.9	F125W	227.9	9
	201.6828	-47.4791	±31	85.9	F139M	502.9	9
	201.6828	-47.4791	±31	85.9	F160W	252.9	9
2010-03-21	201.6828	-47.4791	±31	149.9	F098M	352.9	9
	201.6828	-47.4791	±31	149.9	F110W	227.9	9
	201.6828	-47.4791	±31	149.9.9	F125W	227.9	9
	201.6828	-47.4791	±31	149.9	F139M	502.9	9
	201.6828	-47.4791	±31	149.9	F160W	252.9	9
2010-09-03	201.6828	-47.4791	±31	312.9	F098M	352.9	9
	201.6828	-47.4791	±31	312.9	F110W	227.9	9
	201.6828	-47.4791	±31	312.9.9	F125W	227.9	9
	201.6828	-47.4791	±31	312.9	F139M	502.9	9
	201.6828	-47.4791	±31	312.9	F160W	252.9	9
2010-12-18	201.6828	-47.4791	0	88.62	F105W	227.9	2
	201.6828	-47.4791	0	88.62	F140W	502.9	2
	201.6828	-47.4791	0	88.62	F153M	252.9	2
2011-07-25	201.6828	-47.4791	0	88.62	F105W	227.9	2
	201.6828	-47.4791	0	88.62	F140W	502.9	1
	201.6828	-47.4791	0	88.62	F153M	252.9	1